ATMOSPHERIC SCIENCE LETTERS
Atmos. Sci. Let. **12**: 233–239 (2011)
Published online 17 January 2011 in Wiley Online Library
(wileyonlinelibrary.com) **DOI:** 10.1002/asl.319

RMetS
Royal Meteorological Society

A study of upper troposphere and lower stratosphere water vapor above the Tibetan Plateau using AIRS and MLS data

Wenshou Tian,[1]* Hongying Tian,[1] Sandip Dhomse[2] and Wuhu Feng[2]
[1]*Key Laboratory for Semi-Arid Climate Change of the Ministry of Education, College of Atmospheric Sciences, Lanzhou University, China*
[2]*ICAS, School of Earth and Environment, University of Leeds, UK*

**Correspondence to:*
Wenshou Tian, Key Laboratory for Semi-Arid Climate Change of the Ministry of Education, College of Atmospheric Sciences, Lanzhou University, China.
E-mail: wstian@lzu.edu.cn

Received: 3 September 2010
Revised: 9 November 2010
Accepted: 23 November 2010

Abstract

We use water vapor data from Atmospheric Infrared Sounder (AIRS) and Aura Microwave Limb Sounder (MLS) combined with meteorological data from ECMWF Interim (ERA-Interim) reanalysis, to study some aspects of stratosphere–troposphere exchange (STE) near the Tibetan Plateau. Apart from a distinctive region of high water vapor in the lower stratosphere (LS) in summer near the southern Tibetan Plateau (between 30°N and 35°N), the water vapor in the upper troposphere and lower stratosphere (UTLS) adjacent to the northern Tibetan Plateau (40°N–45°N) is found to be relatively higher than the surrounding regions of the same latitude in March and April. This relatively high water vapor in the northern Tibetan Plateau UTLS is proposed to be associated with approaching cold surges from the north and forced lifting of air by high orography. Another interesting feature detected in this study is the region of low water vapor values on the order of 5–7 ppmv, that is more pronounced from May to September at around 200 hPa and located at 30°N–40°N western Tibetan Plateau. This low water vapor region is found to be related to an anticyclone developed at the western Tibetan Plateau which causes sinking of dry air from the stratosphere resulting lower water vapor values in the upper troposphere.

Keywords: lower stratosphere; water vapor; Tibetan Plateau; stratosphere-troposphere exchange

1. Introduction

Since the discovery of the 'ozone valley' over the Tibetan Plateau (Zhou *et al*., 1995), stratosphere–troposphere exchange (STE) over the Tibetan Plateau has attracted much attention in the scientific community. Increasingly better quality satellite observations have improved our understanding of the effect of the Tibetan Plateau on STE. Among various factors that control STE over the Tibetan Plateau, the convection, monsoon system, air expansion and forced lifting by orography are considered to be important (e.g. Ye and Xu, 2003; Gettelman *et al*., 2004a; Randel and Park, 2006; Liu *et al*., 2009a). Fu *et al*. (2006) pointed out that on a regional scale the Tibetan Plateau provides the main pathway for cross-tropopause transport. Tian *et al*. (2008) and Liu *et al*. (2009b) argued that the STE over the Tibetan Plateau is also closely related to large-scale uplift and descent of isentropic surfaces implied by seasonal and longitudinal variations in the tropopause height.

Using Moderate Resolution Imaging Spectroradiometer (MODIS) data, Chen and Liu (2005) reported two distinct regions over the Tibetan Plateau with large amount of high cirrus clouds: one located over the Indian subcontinent which is linked with the summer monsoon and the other over the Tibetan Plateau which shows a more-or-less standing feature. In their study, Chen and Liu (2005) argued that higher cirrus clouds over the Tibetan Plateau are primarily due to uplifting associated with the cold fronts combined with the topographic forcing. A question arises as to whether those regions with more cirrus clouds correspond to higher water vapor mixing ratios in the lower stratosphere (LS). Although stratospheric water vapor entry mixing ratios are thought to be tightly controlled by tropopause temperature (e.g. Ramaswamy *et al*., 2001; Tian and Chipperfield, 2006; Dhomse *et al*., 2008; Gettelman *et al*., 2009), the spatial variation of the STE over the Tibetan Plateau still remains unclear.

Although the STE just over, or to the south of, the Tibetan Plateau has been studied in detail in previous studies and is linked with the Asian monsoon (e.g. Chen and Liu, 2005; Fu *et al*., 2006; Randel *et al*., 2010), the STE at the northern and western Tibetan Plateau has not been well addressed. In this study, we use measurements from the Atmospheric Infrared Sounder (AIRS) on board Earth Observing System (EOS) Aqua satellite, and the Aura Microwave Limb Sounder (MLS) observations combined with meteorological data from ERA-Interim, to analyze the STE patterns over different regions near the Tibetan

Plateau. Our main objective is to detect important regions for the STE over this region. The satellite and meteorological data used are described briefly in Section 2. Some of key processes and their coupling in controlling the STE are discussed in Section 3, followed by discussion and conclusions in Section 4.

2. Data

The AIRS measurements used in this study are level 3, monthly mean products at 1° × 1° horizontal resolution. We analyze the AIRS water vapor, tropopause pressure and cloud top data for the period from 2003 to 2008. AIRS water vapor mixing ratios are available on 12 standard pressure levels from 1000 to 100 hPa. It is worth noting that although the AIRS data have been extensively validated and are widely used to study transport within the upper troposphere and lower stratosphere (UTLS) region (e.g. Aumann *et al*., 2003; Gettelman *et al*., 2004b; Divakarla *et al*., 2006; Randel and Park, 2006; Xiong *et al*., 2008), AIRS is insensitive to water vapor at less than about 15–20 ppmv (e.g. Read *et al*., 2007). Therefore, the MLS level 2 version 2.2 water vapor data from 2005 to 2008 (e.g. Read *et al*., 2007; Vomel *et al*., 2007) are analyzed together with AIRS data to crosscheck the water vapor distributions in the UTLS region. It has been shown that the MLS v2.2 data have an accuracy better than 25% between 316 and 147 hPa for water vapor mixing ratios less than 500 ppmv (Read *et al*., 2007).

Meteorological data, i.e. temperature, winds and potential vorticity, used are from ECMWF Interim (ERA-Interim) reanalysis for the period from 2003 to 2008 (http://www.ecmwf.int). Although ERA-Interim is available at T255 resolution, here we retrieved ERA-Interim data at the same horizontal resolution as AIRS and MLS data.

3. Results

Figure 1 first shows the 6-year averaged AIRS monthly water vapor mixing ratios at 200 hPa around the Tibetan Plateau. The most noticeable feature is a distinct region of low water vapor over the western Tibetan Plateau at around 30°N–40°N from May to September, and a region of high water vapor located at the southern Tibetan Plateau south of 30°N in summer months. The region of low water vapor values on the order of 5–7 ppmv at 30°N–40°N at the western Tibetan Plateau develops in May and extends westward to about 25 °E from July, and vanishes again in October, while the water vapor around south of 30°N increases gradually from April and reaches a maximum in July and August.

As mentioned above AIRS is insensitive to water vapor at less than about 15–20 ppmv (e.g. Read *et al*., 2007). To further check the validity of these water

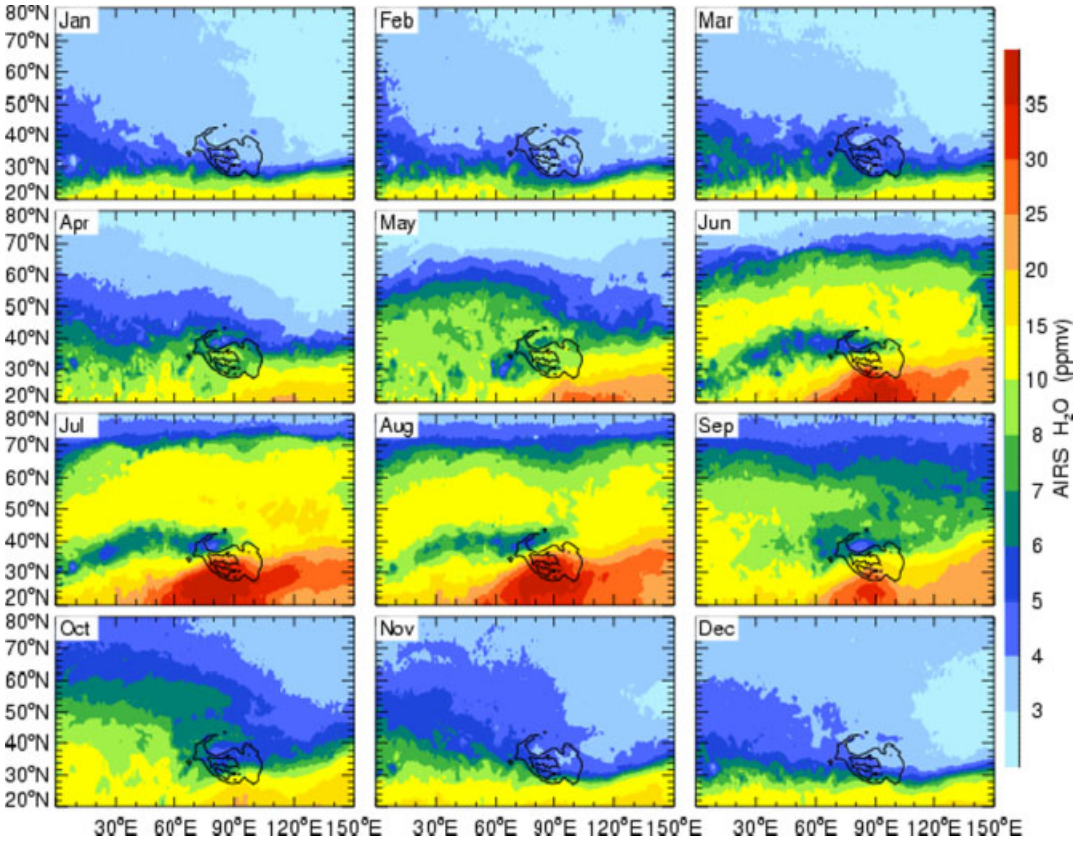

Figure 1. Six-year averaged monthly mean water vapor (ppmv) at 200 hPa from AIRS. The topography of the Tibetan Plateau is denoted by the black solid contours lines with heights above 3 km.

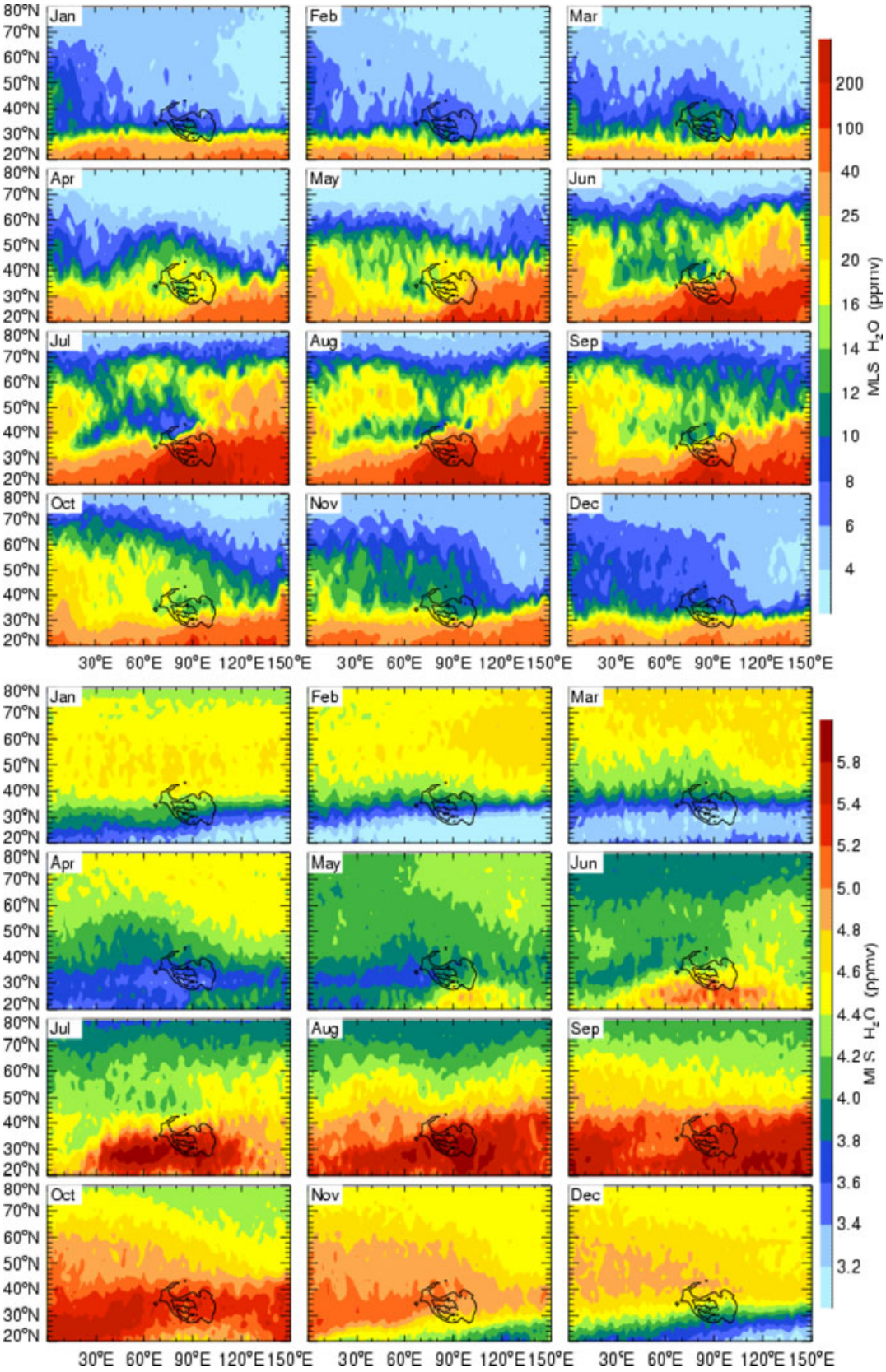

Figure 2. Same as Figure 1, but for 4-years (2005–2008) averaged MLS water vapor data at 215 hPa (top 12 panels) and 100 hPa (bottom 12 panels).

vapor signals in AIRS water vapor, Figure 2 shows the MLS water vapor at 215 hPa. Note that Figure 2 exhibits overall similar features as Figure 1, and the low water vapor values at 30°N–40°N from May to September are also evident. An examination of the AIRS tropopause pressure (not shown) reveals that 200 hPa level is near the tropopause in winter and slightly below the tropopause in summer over

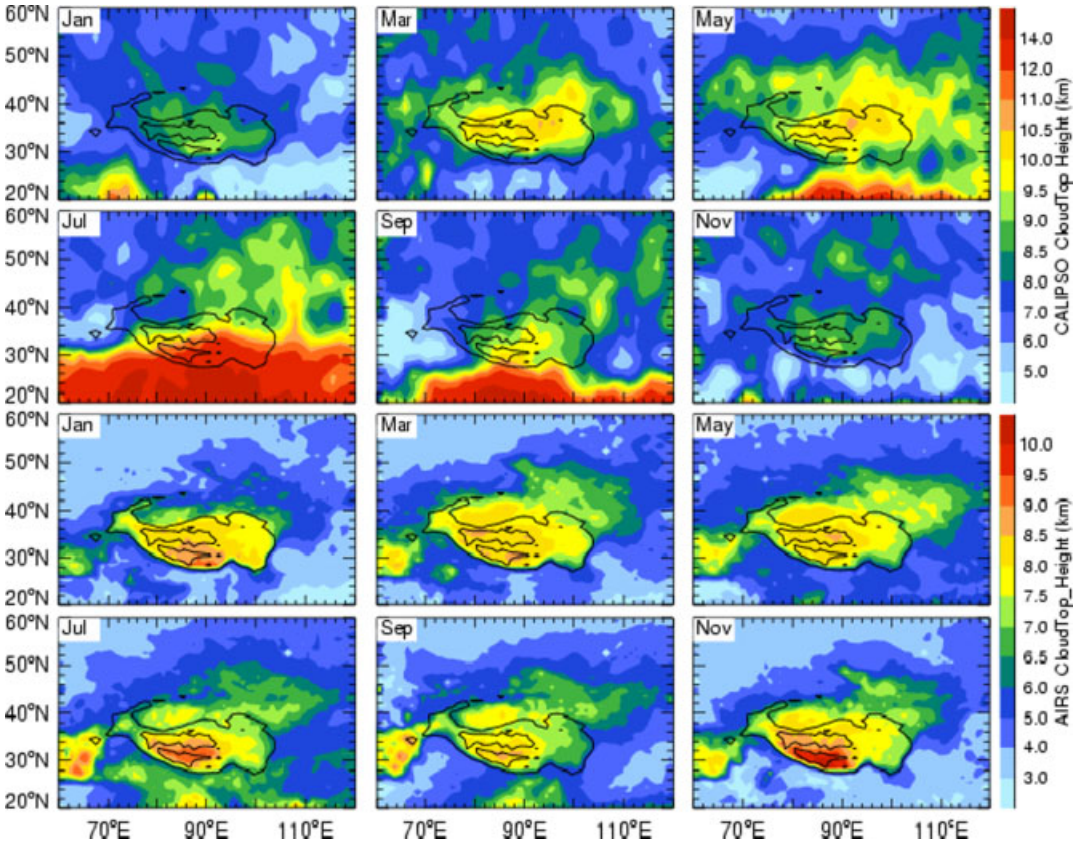

Figure 3. Four-year averaged CALIPSO (top two rows) and 6-year averaged AIRS (bottom two rows) cloud-top height (km) for different months. The data are plotted for every other month. The topography of the Tibetan Plateau is denoted by the black solid contours lines with heights above 3 km.

the Tibetan Plateau, while 100 hPa level well in the stratosphere in winter and spring. In summer, due to thermal heating of the Tibetan Plateau and the development of the monsoon, the tropopause is lifted and reaches a level of around 100 hPa. Therefore, it is necessary to examine the water vapor at 100 hPa which is also shown in Figure 2. Obviously the water vapor distributions at 100 hPa are different from those at 215 hPa. A strong annual cycle can be seen in water vapor at 100 hPa in the south of the Tibetan Plateau with high water vapor values in the summer monsoon season and low values in wintertime. The patches of low water vapor values at 215 hPa at 30°N–40°N seen in Figures 1 and 2 from May to September are not evident at 100 hPa level, but are still visible in May and June.

Further examination of AIRS and MLS water vapor distributions in every individual year from 2005 to 2008 indicates the multi-year averaged results are in accordance with those for every individual year (not shown). Previous studies have pointed out that strong convection and monsoon flow are mainly responsible for the STE over the Tibetan Plateau (e.g. Ye and Xu, 2003; Fu *et al*., 2006; Randel and Park, 2006). Figures 1 and 2 also indicate that high water vapor values, which reach a maximum value of about 6 ppmv in August, over the southern Tibetan Plateau are closely related to the development of the Asian summer monsoon as water vapor maxima in this region increase significantly during summer months when convective activities become intensified.

Figure 3 shows the AIRS cloud top over the Tibetan Plateau as well as the cloud top measured by the Cloud-Aerosol Lidar and Infrared Pathfinder Satellite Observations (CALIPSO) satellite (e.g. McGill *et al*., 2007). We can see that both the AIRS and CALIPSO cloud top over the Tibetan Plateau are about 2 km higher than that over the surrounding area of the same latitude, suggesting the presence of high clouds over the Tibetan Plateau. A more interesting feature in Figure 3 is the high cloud top over the northeastern Tibetan Plateau near 40°N, particularly from March to May. There are no evident high water vapor values around this region at 100 hPa in MLS data. Although there is a distinct region of high water vapor over the northeastern Tibetan Plateau near 40°N in AIRS water vapor data at 100 hPa (not shown), but AIRS data at this level are not robust. A careful examination of MLS water vapor at 215 hPa reveals that water vapor values 40°N north of the Tibetan Plateau are indeed higher than those of the surrounding regions at the same latitude and this feature is particularly evident in February–April. Chen and Liu (2005) pointed out that cirrus clouds over the Tibetan Plateau mostly occur in winter and spring but are nearly absent in summer. CALIPSO cloud top data also show that clouds over the northeastern Tibetan Plateau are obviously higher

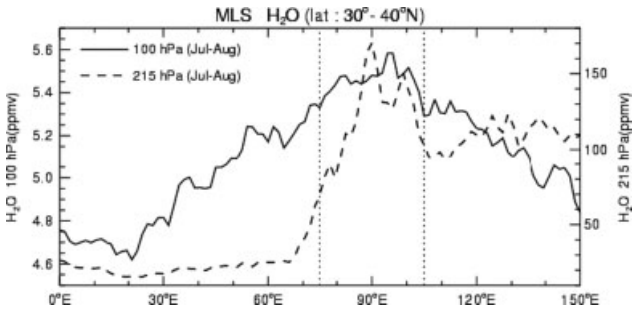

Figure 4. July–August mean MLS water vapor at (solid line) 100 hPa and (dashed line) 215 hPa averaged between latitude 30°N and 40°N. The dotted lines represent the western (75 °E) and eastern (105 °E) boundaries of the Tibetan Plateau.

than those at the surrounding regions of the same latitude from March to May.

Note that a region with high cloud top in the northern Tibetan Plateau also exists from May to September (Figure 3), but there are no evident higher water vapor values at 215 hPa in MLS data. Gao *et al*. (2003) argued that the Hadley circulation is weak in spring over India and the Tibetan Plateau regions. Consequently, there is little dry air from the stratosphere to sink over the Tibetan Plateau. In summer time, the sinking dry air from the stratosphere is strong which prevents the moist air from reaching the tropopause. However, the July–August mean MLS water vapor averaged between latitude band 30°N and 40°N shows that both 100 and 215 hPa water vapor mixing ratios over the northern Tibetan Plateau are higher than those of surrounding longitudes (Figure 4). At 100 hPa, the average water vapor mixing ratio over the Tibetan Plateau (75 °E–105 °E) is 0.50 and 0.30 ppmv higher than that of the western (0–75 °E) and eastern (105 °E–150 °E) Tibetan Plateau, respectively. At 215 hPa, the differences are even larger, and the average water vapor mixing ratio over the Tibetan Plateau is 97 and 12 ppmv higher compared to the western and eastern Tibetan Plateaus, respectively.

A more interesting feature in Figures 1 and 2 is the region of low water vapor values of the order of 5–7 ppmv existing from May to September in the upper troposphere over the western Tibetan Plateau at around 30°N–40°N. This region of low upper tropospheric water vapor is initially located at the western Tibetan Plateau in May and extend westward in June and July, and then retract to the western Tibetan Plateau again in September. To understand the processes and mechanisms responsible for high water vapor values around the northern Tibetan Plateau in spring and the water vapor minima at 30°N–40° from May to September, we analyze the ERA-Interim meteorological data for the same period from 2003 to 2008. Figure 5 shows 6-year averaged wind vectors and temperature fields from January to December at 200 hPa. Also plotted are corresponding potential vorticity fields at 250 hPa for months from October to March and at 225 hPa for months from April to September. Note that 250 and 225 hPa potential vorticity (PV) fields are plotted for different months because the tropopause layer which is delineated by 2.0–3.5 potential vorticity unit (1 PVU $= 1.0\text{E}^{-6}$ m^2 s^{-1} K kg^{-1}) is located just at around 30°N–40°N at 250 hPa from October to March and at 225 hPa from April to September.

The temperature fields in Figure 5 indicate that high water vapor in the region is possibly related to the cold air from the north. It can be seen that cold air pushes southward from north in winter months, and eventually develops a temperature low over the northern Tibetan Plateau in March and April. The cold dry air from the north encounters the warm moist air at the northern edge of the Tibetan Plateau resulting in cold fronts. These cold fronts tend to lift the moist air deep into the upper troposphere and inject the air of tropospheric origin into the stratosphere. During winter and spring, cold surges from north are more frequent and the interaction between cold air and warm air is more likely at around 40°N. On the other hand, in spring, when westerlies encounter the western Tibetan Plateau, they are divided into two branches at around 30°N–40°N and flow around the Tibetan Plateau with a northward branch being the strongest in March and April (Figure 5). Consequently, there is a net transport low PV air from the south to north. Note that in March and April, the 2.0–3.5 PVU surface (implies dynamical tropopause) just located at the western Tibetan Plateau at around 30°N–40°N. Therefore, a net transport of low PV air from the south to north implies a net transport of the tropospheric moist air into the stratosphere at this region. Figures 2 and 3 clearly show that water vapor values over the northern Tibetan Plateau are higher than those of surrounding regions at the same latitude in March and April.

The wind and temperature fields together with PV fields over and surrounding the Tibetan Plateau suggest a mechanism for water vapor minima in the upper troposphere from May to September at 30°N–40°N. From May to September, a warm center develops around the Tibetan Plateau. Associated with this warm center, we can see an evident anticyclone appears in May at the western Tibetan Plateau and it becomes strongest in July and August and extends westward to about 25 °E. The anticyclone retracts from August and eventually disappears after September when the warm center no longer exists. This anticyclone causes a sinking of dry air from the above and results in low water vapor values at around 30°N–40°N at the western Tibetan Plateau from May to September. It is apparent that the development of this anticyclone is accompanied by a warm center around the Tibetan Plateau from May to September (Figure 5), while the spatial and temporal variations of this low water vapor region in Figures 1 and 2 are in a good accordance with the development of this anticyclone.

It is possible that other processes like tropopause fold events are also responsible for the dry band over the west of the Tibetan Plateau during the summer months. The diabatic heating associated with

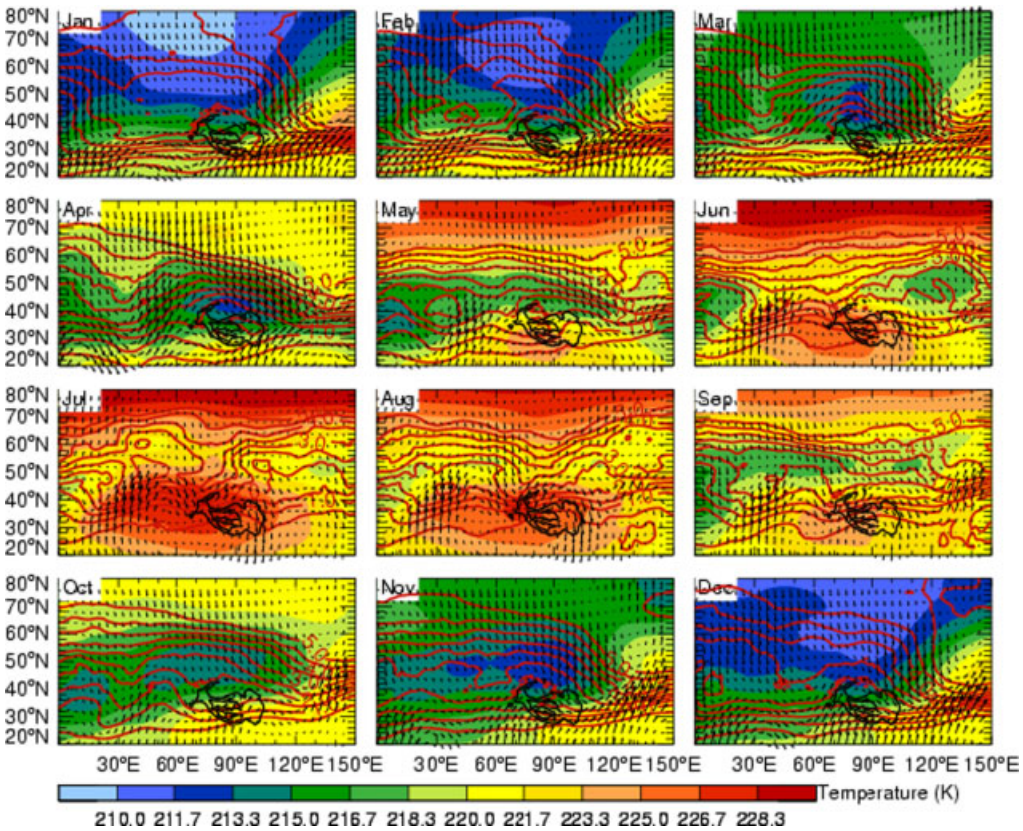

Figure 5. Six-year averaged ECMWF (ERA-Interim) temperature (K, filled contours), wind vectors at 200 hPa for all months. To make the wind vectors more visible over the Tibetan Plateau, the zonal wind component is divided by a factor 10. Potential vorticity (PV) fields at 250 hPa (for October–March) and 225 hPa (for April–September) are shown with red contour lines. Contour interval for the PV fields is 0.5 PVU (1 PVU = $1.0E^{-6}$ m^2 s^{-1} K kg^{-1}).

strong convective activities over this region in summer may have an impact on the STE and hence on the water vapor distribution in the UTLS region. Further investigation on this issue using the data with higher spatial and temporal resolution is worthwhile.

4. Discussion and Conclusions

We have used the high resolution MLS and AIRS measurements together with ERA-Interim meteorological data to analyze water vapor in the lower stratosphere near the Tibetan Plateau. The high water vapor in the UTLS at the southern Tibetan Plateau is more pronounced in summer due to the monsoon-induced stronger upward motions. This feature is in agreement with earlier studies. We report that water vapor mixing ratios in the UTLS at the northern Tibetan Plateau in March and April are also relatively higher than those at surrounding regions of the same latitude. The relatively high water vapor at the northern Tibetan Plateau is proposed to be related to cold surges from north and associated cold fronts together with orographic lifting of air at the northern edge of the Tibetan Plateau.

A more interesting feature detected in this study is a region of low water vapor values on the order of 5–7 ppmv existing from May to September in the upper troposphere at around 200 hPa over the western Tibetan Plateau. This low water vapor region is located at 30°N–40°N and extended westward to a longitude of 25 °E in August. The analysis of the corresponding meteorological fields reveals that the low water vapor in the upper troposphere is related to an anticyclone developed at the western Tibetan Plateau which causes a sinking of dry air from the UTLS region and results in low water vapor values in the upper troposphere.

Acknowledgements

This work was supported by the National Science Foundation of China (40730949) and National Basic Research Program of China (2010CB428604). We thank the AIRS and MLS teams for water vapor and other data, particularly Dr Edward Olsen for help in processing and interpreting the data and Prof. Martyn Chipperfield for helpful comments. WT is also thankful to ECMWF for meteorological data and the School of Earth and Environment, University of Leeds, for computing support. We thank two anonymous reviewers for their helpful comments which significantly improved the quality of this article.

References

Aumann HH, Chahine MT, Gautier C, Goldberg MD, Kalnay E, McMillin LM, Revercomb H, Rosenkranz PW, Smith WL, Staelin DH, Strow LL, Susskind J. 2003. AIRS/AMSU/HSB on the Aqua mission: design, science objectives, data products, and processing systems. *IEEE Transactions on Geosciences and Remote Sensing* **41**(2): 253–264.

Chen B, Liu X. 2005. Seasonal migration of cirrus clouds over the Asian monsoon regions and the Tibetan Plateau measured from MODIS/Terra. *Geophysical Research Letter* **32**: L01804, DOI:10.1029/2004GL020868.

Dhomse S, Weber M, Burrows J. 2008. The relationship between tropospheric wave forcing and tropical lower stratospheric water vapor. *Atmospheric Chemistry and Physics* **8**: 471–480.

Divakarla MG, Barnet CD, Goldberg MD, McMillian LM, Maddy E, Wolf W, Zhou L. 2006. Validation of AIRS temperature and water vapor retrievals with matched radiosonde observations and forecasts. *Journal of Geophysical Research* **111**(D09S15): 20.

Fu R, Hu Y, Wright JS, Jiang JH, Dickinson RE, Chen M, Filipiak M, Read WG, Waters JW, Wu DL. 2006. Short circuit of water vapour and polluted air to the global stratosphere by convective transport over the Tibetan Plateau. *PNAS* **103**: 5664–5669.

Gao B, Yang P, Guo G, Park SK, Wiscombe WJ, Chen B. 2003. Measurements of water vapor and high clouds over the Tibetan Plateau with the Terra MODIS instrument. *IEEE Transactions on Geosciences and Remote Sensing* **41**((4)): 895–900.

Gettelman A, Birner T, Eyring V, Akiyoshi H, Bekki S, Bruehl C, Dameris M, Kinnison DE, Lefevre F, Lott F, Mancini E, Pitari G, Plummer DA, Rozanov E, Shibata K, Stenke A, Struthers H, Tian W. 2009. The tropical tropopause layer 1960–2100. *Atmospheric Chemistry and Physics* **9**: 1621–1637.

Gettelman A, Kinnison DE, Dunkerton TJ, Brasseuret GP. 2004a. Impact of monsoon circulations on the upper troposphere and lower stratosphere. *Journal of Geophysical Research* **109**: D22101, DOI:10. 1029/2004JD004878.

Gettelman A, Weinstock EM, Fetzer EJ, *et al*. 2004b. Validation of Aqua satellite data in the upper troposphere and lower stratosphere with in situ aircraft instruments. *Geophysical Research Letter* **31**: L22107, DOI:10.1029/2004GL020730.

Liu C, Liu Y, Cai Z, Gao S, Lü D, Kyrö lä E. 2009a. A Madden–Julian oscillation-triggered record ozone minimum over the Tibetan Plateau in December 2003 and its association with stratospheric "'low-ozone pockets"'. *Geophysical Research Letter* **36**: L15830, DOI:10.1029/2009GL039025.

Liu Y, Wang Y, Liu X, Cai Z, Chance K. 2009b. Tibetan middle tropospheric ozone minimum in June discovered from GOME observations. *Geophysical Research Letter* **36**: L05814, DOI:10.1029/2008GL037056.

McGill ML, Vaughan MA, Trepte CR, Hart WD, Hlavka DL, Winker DM, Kuehn R. 2007. Airborne validation of spatial properties measured by the CALIPSO lidar. *Journal of Geophysical Research* **112**: D20201, DOI:10. 1029/2007JD008768.

Randel W, Park M. 2006. Deep convective influence on the Asian summer monsoon anticyclone and associated tracer variability observed with Atmospheric Infrared Sounder (AIRS). *Journal of Geophysical Research* **111**: D12314, DOI:10.1029/2005JD006490.

Randel WJ, Park M, Emmons L, Kinnison D, Bernath P, Walker KA, Boone C, Pumphrey H. 2010. Asian monsoon transport of pollution to the stratosphere. *Science* **328**: DOI: 10.1126/science.1182274.

Read WG, Lambert A, Bacmeister J, Cofield RE, Christensen LE, Cuddy DT, Daffer WH, Drouin BJ, Fetzer E, Froidevaux L, Fuller R, Herman R, Jarnot RF, Jiang JH, Jiang YB, Kelly K, Knosp BW, Kovalenko LJ, Livesey NJ, Liu HC, Manney GL, Pickett HM, Pumphrey HC, Rosenlof KH, Sabounchi X, Santee ML, Schwartz MJ, Snyder WV, Stek PC, Su H, Takacs LL, Thurstans RP, Vömel H, Wagner PA, Waters JW, Webster CR, Weinstock EM, Wu DL. 2007. Aura Microwave Limb Sounder upper tropospheric and lower stratospheric H_2O and relative humidity with respect to ice validation. *Journal of Geophysical Research* **112**: D24S35, DOI:10.1029/2007JD008752.

Ramaswamy V, Chanin ML, Angell J, Barnett J, Gaffen D, Gelman M, Keckhut P, Koshelkov Y, Labitzke K, Lin JJR, O'Neill A, Nash J, Randel W, Rood R, Shine K, Shiotani M, Swinbank R. 2001. Stratospheric temperature trends: observations and model simulations. *Review Geophysics* **39**: 71–122.

Tian WS, Chipperfield MP. 2006. Stratospheric water vapor trends in a coupled chemistry-climate model. *Geophysical Research Letter* **33**: L06819, DOI:10.1029/2005GL024675.

Tian W, Chipperfield MP, Huang G. 2008. Effects of the Tibetan Plateau on total column ozone distribution. *Tellus* **60B**: 622–636.

Vomel H, Barnes JE, Forno RN, Fujiwara M, Hasebe F, Iwasaki S, Kivi R, Komala N, Kyrö E, Leblanc T, Morel B, Ogino SY, Read WG, Ryan SC, Saraspriya S, Selkirk H, Shiotani M, Valverde Canossa J, Whiteman DN. 2007. Validation of Aura Microwave Limb Sounder water vapor by balloon borne Cryogenic Frost point Hygrometer measurements. *Journal of Geophysical Research* **112**: D24S37, DOI:10.1029/2007JD008698.

Xiong X, Barnet C, Maddy E, Sweeney C, Liu X, Zhou L, Goldberg M. 2008. Characterization and validation of methane products from the Atmospheric Infrared Sounder (AIRS). *Journal of Geophysical Research* **113**: G00A01, DOI:10.1029/2007JG000500.

Ye Z, Xu Y. 2003. Climate characteristics of ozone over Tibetan Plateau. *Journal of Geophysical Research* **108**(D20): 4654.

Zhou X, Lou C, Li WL, Shi JE. 1995. Ozone changes over China and low center over Tibetan Plateau. *Chinese Science Bulletin* **40**: 1396–1398.